Progressive Failure of Undercut Backfilled Stopes: the Problem with Mitchell's Sill Mat Analysis

Murray W. Grabinsky[1] and Ben D. Thompson[1]

[1]Paterson & Cooke, Sudbury, ON, Canada, murray.grabinsky@patersoncooke.com

Abstract

Many practitioners use Mitchell's (1991) method to assess backfill strength requirements for stability of undercut backfills, or other empirical methods motivated by Mitchell's approach. There are, however, case histories of stable undercut backfill with strengths significantly less than the assessed strength requirements from these methods. Here, we consider the case of vertical orebodies and use a systematic numerical investigation to show that Mitchell's method only captures the first stage of a stable progressive failure mechanism. Subsequent failure stages depend in part on the assumed backfill strength criterion, but recent laboratory investigations of direct tensile strength and compressive strengths under low confining stress are used to constrain the most likely subsequent failure modes and their corresponding imposed stress levels. The results can be normalized in terms of two ratios: 1) backfill Unconfined Compressive Strength (UCS) to driving stresses (self weight and imposed loads); and 2) the undercut span (L) to depth (d) of the backfill sill mat (also called the plug, or backfilled drift, depending on the design context). Numerical modelling, Mitchell's equations, and empirical approaches give a similar required strength assessment for $L/d \sim 1.0$, but the results progressively diverge as L/d increases with the modelling approach giving the lowest strength assessments. Notably, the assessed strengths from modelling are consistent with the lowest values found in published case histories. Also, the modelling results indicate that flexure is always the critical failure mode; the other failure modes postulated by Mitchell (sidewall sliding and tensile caving) do not manifest in the numerical modelling results. While modelling in this study has some restrictive assumptions (ie, vertical orebodies, no rock mass closure), the results explain why previous design methods appear to over-estimate strength requirements, particularly for backfills with large undercut span to backfill depth (L/d) ratios.

Key words: design strength, underhand cut and fill (UCF), backfill plug, numerical analysis.

Introduction

Mining with backfill enables an operation to maximise orebody extraction, with backfill strength being engineered to allow exposures of backfill to remain stable following mining of adjacent stopes. The most common design occurrence is vertical backfill exposures. Many operations also mine under backfill, whether that be cases of a mining block expanding up to meet a previously backfilled level, or the 'underhand' cut and fill case where ground control risk management makes mining under previously placed backfill the preferred solution. In these undercut cases, there is a need to define backfill strength to enable the backfill sills to remain stable as the horizontal backfill plane is exposed. Undercut backfill design scenarios are summarized (Figure 1) for both longhole and cut and fill stoping methods.

Determining required backfill strength to safely undercut previously placed backfill is arguably one of the most difficult and contentious backfill design challenges. Mitchell (1991) appears to have been the first to propose a rational analysis method for such designs, albeit using the terminology of 'sill mat' which was

"...often cast from cemented backfill materials, usually without reinforcements but often underlain by a timber mat." Four independently assessed potential failure modes were proposed: flexure, caving, block shear, and rotation. A fifth mode, backfill crushing, was earlier proposed by Mitchell and Roettger (1989), but is notably absent in the 1991 article. For shallow-dipping orebodie,s the rotational failure mode was suggested as generally being most critical. For sub-vertical orebodies, many investigators find the flexural failure mode to dominate (eg, Raffaldi et al., 2019). However, theoretical determination of the critical mode will depend in part on the backfill geometry but also on the assumed failure envelope (or failure criterion) for the backfill's intact strength, and on the contact strength between the backfill and the sidewall material (host rock or previously placed backfill). As well, Mitchell and Roettger (1989) considered the possibility of sidewall closure upon undercutting, which if small could contribute to stability in the flexural failure mode, but if large could contribute to instability in the crushing failure mode.

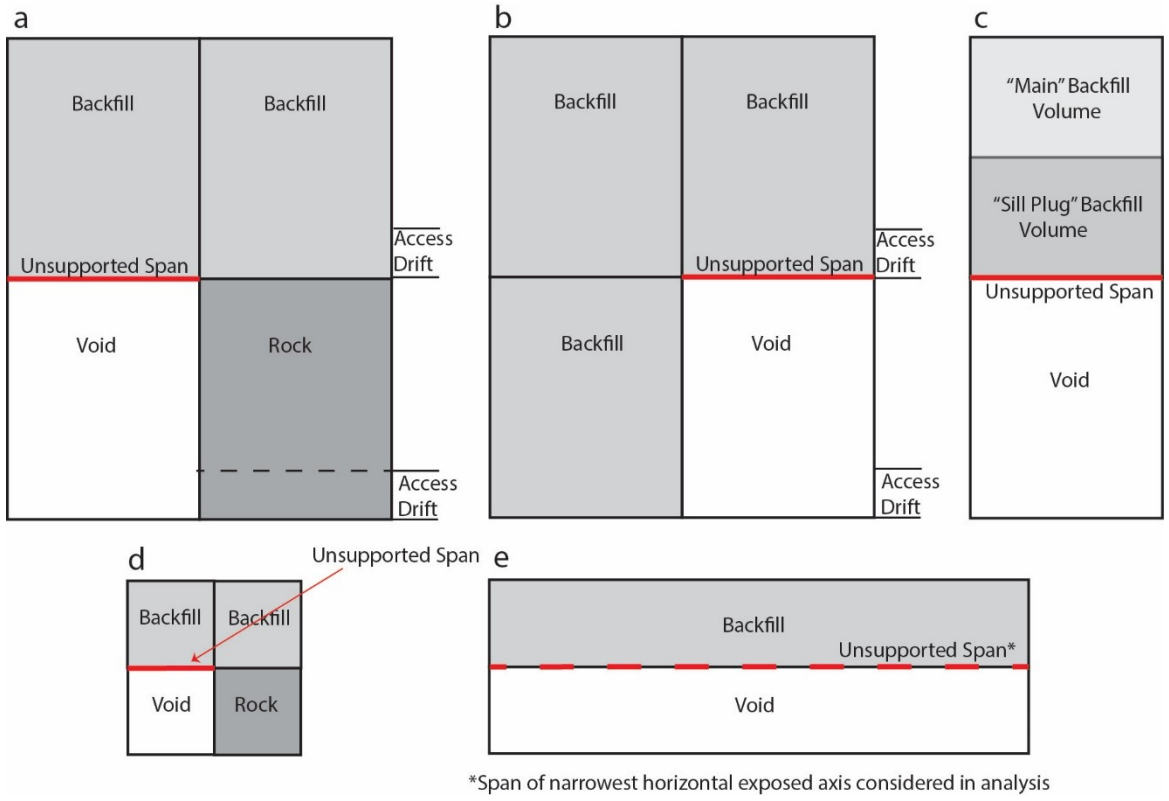

Figure 1. Simplified design scenarios resulting in undercut exposures of backfill, (a) and (b) show cross section views of longhole stoping cases with (c) defining terminology. In d) and e), underhand cut and fill stoping is shown with section views into the plane of short and long horizontal axes, respectively.

Understandably, given the range of Mitchell's proposed possible failure modes and uncertainties regarding the appropriate intact and contact strength criteria, practitioners have sought more practical approaches for undercut backfill strength assessment. This was further motivated by Mitchell's method

often producing assessed strengths that seemed unrealistically high and inconsistent with mining experience, suggesting an element of empirical modification was required.

Stone (1993) developed a design chart for the required strength of undercut Cemented Rock Fill (CRF) based on the Mitchell and Roetterger (1989) flexural failure criterion, although formulation of the design curves was not provided. Stone noted that the chart was verified by physical (centrifuge models) and empirical (comparison with mine exposure) methods. Pakalnis et al, (2005) adapted Stone's design chart approach by including a database of undercut case histories (updated by Pakalnis, 2015) and presenting these along with a series of 'empirical' design curves. It is possible to reconstruct those design curves using reasonable input parameter assumptions. As discussed in Grabinsky et al. (2022), the most significant deviation from the Mitchell flexure criterion is critical stress concentration dependence on $\left(\frac{d}{L}\right)^{1.5}$ instead of $\left(\frac{d}{L}\right)^{2}$, where L is the undercut span and d is the depth of the backfill component (ie, the height of the backfilled drift in the case of underhand cut-and-fill mining, or the 'plug' or sill mat height in the case of mining methods using large open stopes). The correspondence of the case histories and the design curves in Pakalnis et al. (2005) can be misleading, however, as the Pakalnis chart implies all case histories have an assessed Strength Factor of 2.0. Grabinsky et al. (2022) reinterpreted the Pakalnis et al (2005) data and replotted it, showing that the case histories had assessed Strength Factors ranging from < 1.5 to > 8. It is reasonable to say, therefore, that although these design tools have significant benefit as evidenced by decades of widespread use, continued improvement is feasible and justified in terms of recognizing existing limitations and providing more efficient design solutions. This paper aims to provide interpretation of recent numerical analysis to better understand where potential efficiencies exist, and how numerical modelling approaches can provide the basis of practical design.

Analysis approach

To better understand backfill behaviour when it is undercut, the modelling approach considered next follows the methodology proposed by Starfield and Cundall (1988) for design problems that are data limited, and lack a fundamental understanding of the governing system mechanics. Specifically, the starting point is a relatively restrictive system idealization (ie, vertical orebody and no sidewall closure), to minimize complexity. Next, we constrain the idealized material behaviour based on the best available testing data and parameterize it to facilitate subsequent attempts to determine normalized solutions using dimensionless parameters.

We then develop an initial model that performs 'exactly' to a problem analogue for which a mathematical solution exists. This establishes a reliable estimate of the onset of progressive failure. Nonlinear analysis then follows, with subsequent progressive failure stages being determined in an unbiased way by the model based solely on the starting assumptions about geometry, material properties, and boundary conditions. Parameters are then varied to develop a general solution to the idealized system behaviour. These results are then compared with available case history data. The outcome of this process should indicate where the results can be used reliably, and where the approach may need to be extended to address the original simplifications and incorporate more realistic assumptions for increasingly challenging design scenarios.

Initial system idealization

The flexure criterion suggested by Mitchell was motivated by the solution for a uniformly loaded, fixed-fixed (encastered) beam. Unlike a simply supported beam where the maximum moment, M_o, occurs at the centre span, for a fixed-fixed beam the bending moment diagram is shifted so that the maximum (absolute) value is $\frac{-2}{3}M_o$ at either end of the beam, and $\frac{1}{3}M_o$ at the center span. The negative moment at the fixed ends implies maximum tensile normal stress at the top corners and maximum compressive normal stresses at the bottom corners. Given that cemented backfill is weaker in tension than in compression, the critical stress concentration is therefore at the top end corners. Mitchell expressed the corresponding failure criterion as follows:

$$\left(\frac{L}{d}\right)^2 > 2\left(\sigma_t + \sigma_c\right)/w \qquad \text{Equation 1}$$

Where L and d are the backfill dimensions as defined previously, w is the uniformly distributed load which includes the backfill's self weight, σ_c is the 'clamping stress' arising from sidewall closure (and will be ignored in the present work), and σ_t is the material's tensile strength. For a compression positive sign convention, clamping stress will be a positive value and tensile strength will be a negative value.

Many works (eg, Pakalnis et al., 2005) based on Equation 1 assume that the tensile strength is UCS/10. There are two problems with this assumption. First, the tensile strength that should be used with Equation 1 is the *contact* tensile strength between the backfill and the sidewall material against which the backfill is poured and cured. Invariably, the contact tensile strength is found to be less than the *intact* tensile strength, which is also the case for cold joints if backfill is not poured continuously. Second, the assumption of UCS/10 probably comes from rock mechanics, but this is a generalization of findings from intact rock testing. Indeed, for intact rock classifications that may be considered similar to Cemented Paste Backfill (CPB) the ratio is more likely in the range 1/3 to 1/6. Grabinsky et al. (2022) review tensile stress test results from various sources which use different test techniques and suggest a recent form of Direct Tensile (DT) test method is most appropriate, with reported values for CPB lying in the range UCS/3 to UCS/5.

Whatever reasonable contact tensile strength might be assumed, *the fundamental problem with using Equation 1 as a 'failure criterion' is that it only predicts the onset of failure at the top sidewall corners*, and the initial failure at these locations does not imply structural collapse. As the driving stress, w, keeps increasing, the sidewall cracking will propagate downward and the internal compressive stresses within the backfill 'beam' will readjust to enhance arching between the remaining sidewall areas that remain in compression (ie, closer to the bottom sidewall corners). No analytic solution exists to predict this progressive failure process exactly, and so numerical modelling is required.

Assessing the subsequent stages of progressive failure and determining which becomes critical will depend in large part on the assumed material properties, particularly the strength envelope. It is therefore important to use realistic strength assumptions.

Idealized backfill material behaviour

When assessing the frictional strength of geomaterials, a conventional approach is to use triaxial tests to capture the effect of confining stress. However, normal laboratory testing conditions imply this will typically result in normal stresses acting on the conjugate shear planes of failure that are much higher than would be expected to act within in a CPB beam (as will be shown later). Figure 2 shows an example strength envelope determined for Williams mine CPB (Grabinsky et al., 2022). The Mohr-Coulomb failure envelope is conventionally determined by finding the tangents to the corresponding Mohr's circles at failure, in this case for UCS and DT tests. It is a useful observation that the stress points representing the failure condition determined from Direct Shear (DS) tests are consistent with this failure envelope suggesting greater use of these relatively inexpensive tests may be justified. The confining stresses for the individual DS tests were varied from 0 (which then gives the cohesion, *c*) to less than ½ UCS.

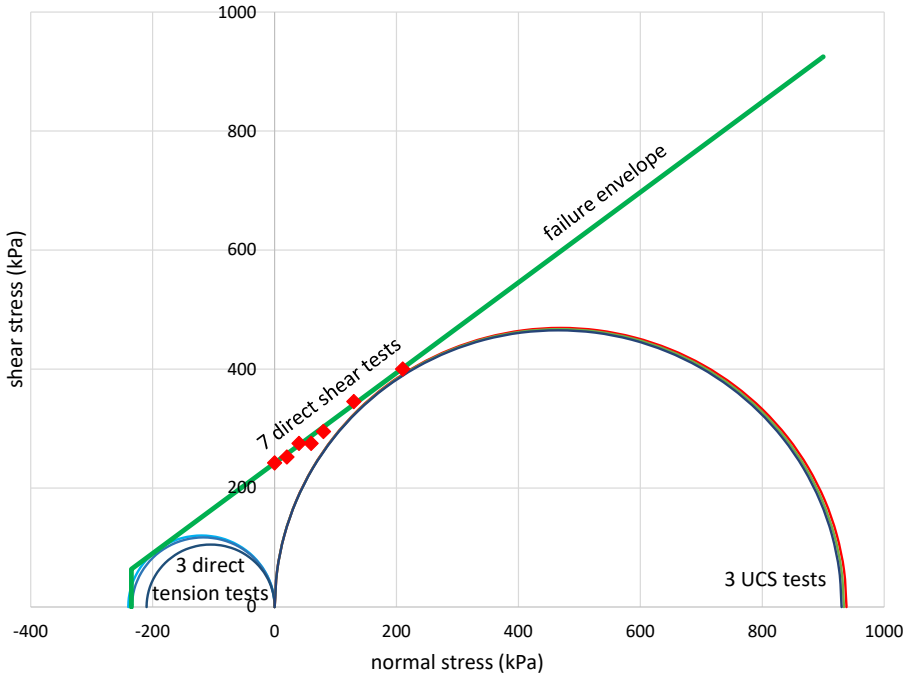

Figure 2. Failure envelope for Williams CPB determined using UCS, DS, and DT methods

It can be observed that the DS failure condition for the highest confining stress value used corresponds with the tangent of the UCS Mohr's circle to the failure envelope, thereby confirming the consistency of the individual test methods. For the data shown the friction angle is determined to be 37° for ¼ UCS. This value of friction angle is often reported from tests on other CPB materials (Grabinsky et al., 2022) and is consistent with that determined from tests on many non-plastic tailings (Vick, 1990).

As mentioned previously, the contact tensile strength will be less than the intact tensile strength, but this has not been extensively investigated. If UCS/4, then a contact tensile strength of UCS/10–UCS/20 is arguably reasonable and will be used in subsequent numerical modelling.

While elastic parameters are not used in Equation 1, they are needed for numerical modelling. Grabinsky et al. (2022) consider a wide range of published results from UCS tests, reproduced in Figure 3. Generally, the tangent Young's Modulus varies from about 10^2 to 10^3 × UCS. Numerical modelling results showed little sensitivity to Poisson's ratio values between 0.2–0.3.

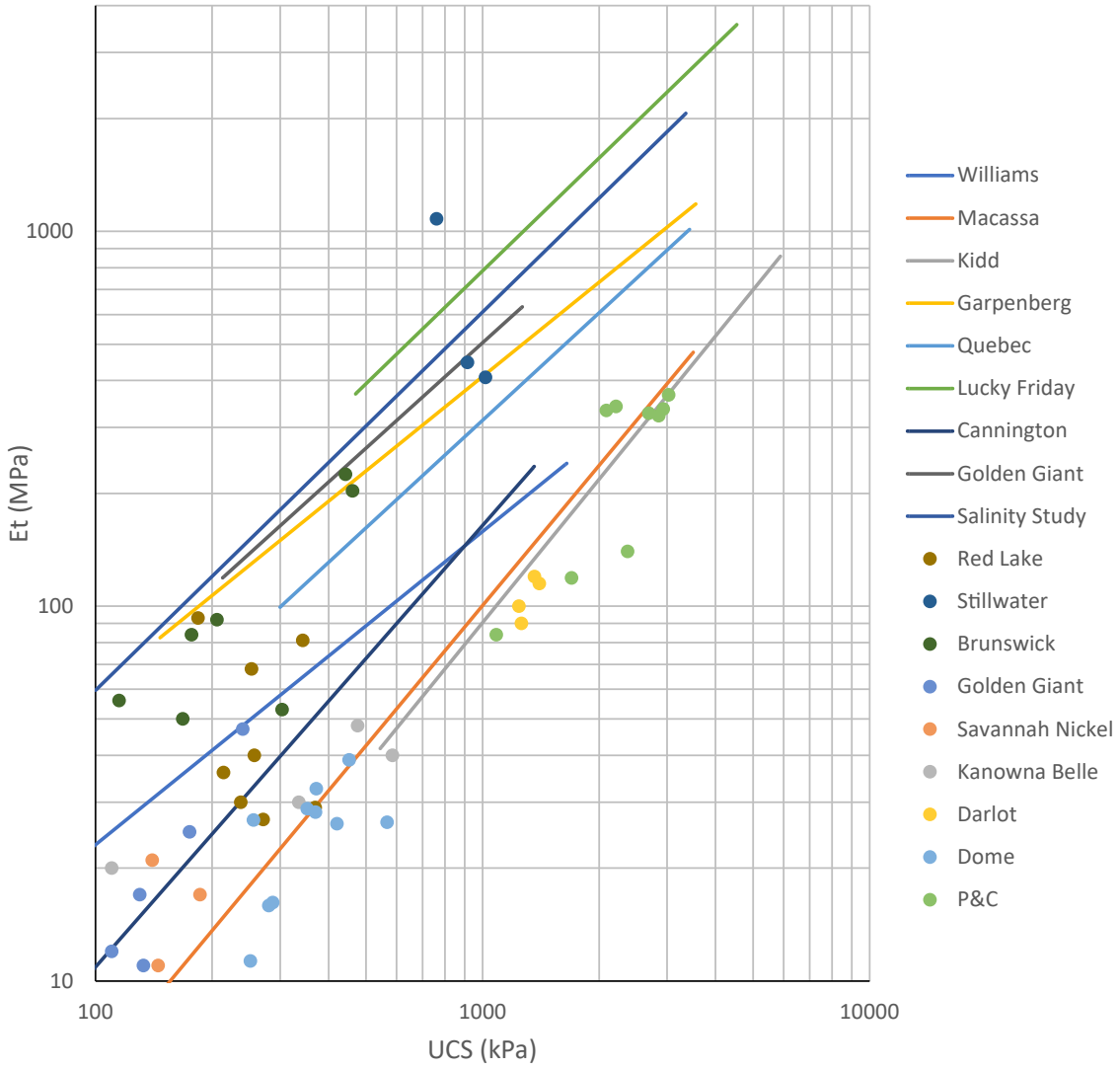

Figure 3. Correlations between tangent Young's Modulus and UCS from published results; with data points (dots) and best fit lines included, as described in Grabinsky et al., (2022).

Numerical model calibration and progressive failure simulation

The contact behaviour between the backfill material and the sidewalls is critical when considering analysis of undercut backfill stability, thus numerical modelling must pay particular attention to this area. The most effective modelling approach is to use special joint elements along this contact. In this model calibration stage, the joint's "elastic" properties (ie, normal and shear stiffnesses) must reproduce Mitchell's tensile stress concentrations at the upper corners when the analysis remains elastic, with no joint failure. For subsequent nonlinear analysis the joint's tensile failure criterion should be less than the intact tensile strength, and values of UCS/10 and UCS/20 are investigated here as part of a sensitivity analysis. It is assumed here that the sidewalls have roughness with undulation amplitudes larger than the largest particle size of the backfill and that sidewall materials are stronger than the backfill; therefore, shear failure must occur through the backfill and the joint's shear strength parameters are equivalent to the backfill's internal shear strength parameters. This is consistent with recent laboratory test results (Yang et al., 2024) where backfill was cast against rock with notches only 2 mm deep (corresponding to a JRC ~ 8) and direct shear tests confirmed that the interface retained the shear strength of the original intact material.

The commonly used commercially available nonlinear finite element (or finite difference) programs for geomechanics applications generally contain joint elements, although their implementation varies. It is important that practitioners trying to replicate the approach recommended here be completely familiar with the theoretical basis of a program's joint elements and conduct simplified tests to verify they are being used as intended. Modelling results shown here were conducted with the 2D finite element code RS2 from Rocscience Inc. An example model for a nonlinear analysis of undercut paste stability is shown in Figure 4. The modelling approach is described as follows:

1. The beam is modelled as symmetric with 'roller' boundary conditions along the left-hand side, representing beam center span.
2. The meshes consisted of six-nodded triangular elements, numbering from a few thousand to 15,000 depending on the span.
3. The sidewall material is modelled as elastic with a Young's Modulus at least 10^6 × the backfill material's modulus, and its outer boundaries are rigid.
4. The beam has unit weight 20 kN/m^3 and gravitational loading is applied, along with an initial geostatic stress field condition using a horizontal to vertical stress ratio of 0.25. This stress ratio is based on field experimental results and discussed in our companion paper (Grabinsky et al., 2024).
5. The initial model is elastic (including the joint, ie, no tensile failure) and the normal stress distribution along the contact is checked to assess the tensile stress concentration at the top corner.
6. Joint stiffness is adjusted to produce the correct concentration according to Equation 1.

This is a rapidly convergent iterative process. Clearly, a reasonable design should maintain a SF) > 1, and so the beam can be modelled as elastic, while the nonlinearity lies in the joint response. The results presented here assume a 37° friction angle and so the cohesion and intact tensile strength are ¼ UCS.

An upper-bound UCS is obtained from Equation 1 representing the elastic tensile concentration, and then UCS is progressively reduced so that the tensile cracking down the sidewall increases in length and the SF proximate to the tip of this crack decreases. The SF is displayed graphically as a contour plot from the

modelling package. When the SF reaches the desired minimum value (SF = 2.0 as consistent with the assumption of previously described empirical methods of Stone and Palaknis) the iteration stops and convergence to the minimum required UCS is achieved.

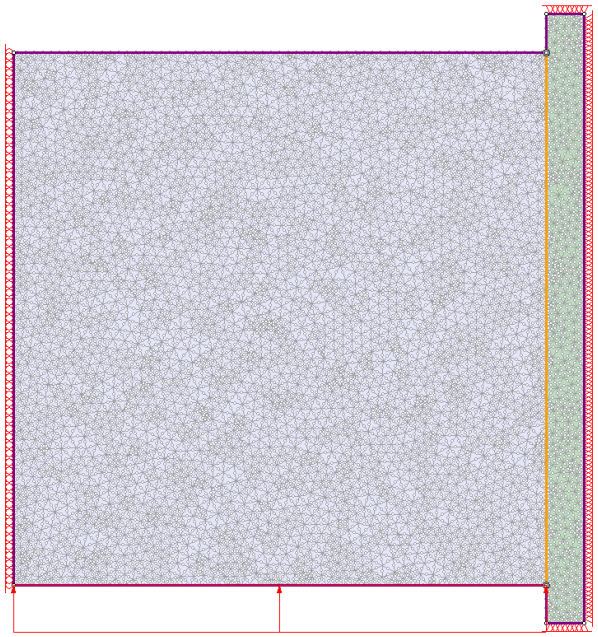

Figure 4. Example numerical model; left roller boundary condition to simulate symmetry; primary backfill 'beam' (grey); interface joint (vertical orange line); stiff host rock (green); right rigid boundary condition (triangle markers); and initial stabilizing pressure beneath the beam (red arrow block).

On each of these nonlinear runs there is an initial stage with a bottom pressure equal to γd so that results at this stage can be checked to ensure the model is in equilibrium (ie, there is no deformation of the bottom surface). The bottom pressure is then reduced to zero in ten equal stages, which permits more detailed examination of results and interpretation of the progressive failure mechanisms.

Figure 5 shows a backfill beam with aspect ratio 1.5 and demonstrates how the progressive failure takes place along the sidewall (failed joints are shown as red lines) as the initial supporting pressure along the beam's lower surface is reduced. The dark blue lines are trajectories of major principal compressive stress, and the contours are blue for lowest stress and red for highest stress, but magnitudes are not shown because these will scale with the absolute size of the beam. The final, 'unsupported' figure shows the internal arching mechanism developed.

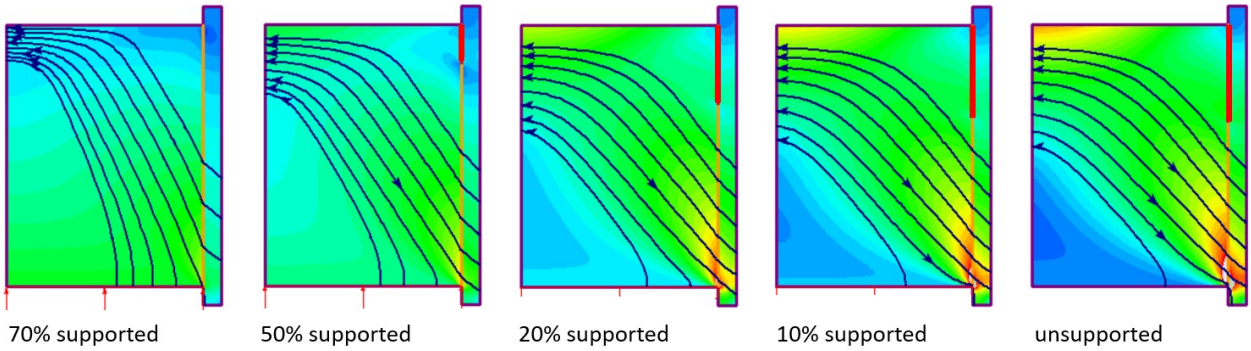

Figure 5. Progressive failure with reduction of supporting pressure under the backfill beam: the curved lines indicate the flow of major compressive stress within the beam; and the red lines show progressive contact interface (joint) failure as the bottom supporting pressure is reduced.

An important clarification in terms of interpreting subsequent results considers SF at the bottom centre span, where the stresses are tensile, compared with SF near the crack tip (ie, joint locations coloured red) where the major principal stress is compressive and the minor principal stress is much closer to the unconfined condition. Tensile stress at the bottom centre span would lead to vertical cracking which would quickly propagate into a compressive region and stabilize, so the sidewall condition is considered the primary area of concern. It must also be noted that SF plots generated using other finite element programs may not produce exactly the same contours, because RS2 defines SF based on maximum shear and mean stress, whereas other programs typically use the maximum and minimum principal stresses.

Results generalization

Because the beam itself is elastic, the subsequent numerical analysis results can be normalized as follows. The beam's aspect ratio, $\left(\frac{L}{d}\right)$, controls the extent of sidewall cracking with relatively thick beams having little or no sidewall cracking, and relatively slender beams having the greatest extent of sidewall cracking. The ratio of strength to driving stress can be normalized as $\left(\frac{UCS}{\gamma d}\right)$. In rock mechanics it is conventional to express the relationship between tensile and unconfined compressive strengths as $UCS = m\,\sigma_t$ in (ie, m is the ratio of compressive to tensile uniaxial strengths) in which case Equation 1 can be expressed in normalized form as Equation 2:

$$SF\,\frac{m}{2}\left(\frac{L}{d}\right)^2 = \left(\frac{UCS}{\gamma d}\right) \qquad \text{Equation 2}$$

Note that Equation 2 is unreasonable for very thick beams because when $d \gg L$ the required strength goes to zero.

The modelling approach described in the previous section was carried out for a range of beam aspect ratios from 0.25–4.5. Figure 6 shows the sensitivity of the crack penetration depth (ie, the length of the red lines shown in relative to the beam depth, and of the normalized strength, $\left(\frac{UCS}{\gamma d}\right)$, to the aspect ratio, $\left(\frac{L}{d}\right)$, assuming the contact tensile strength is either UCS/10 or UCS/20.

Critically, *the normalized strength is unaffected for assumed contact tensile strengths within this range*. Note that sidewall cracking only occurs for aspect ratios > 1 when the assumed contact tensile strength is UCS/10. For the range of contact strengths assumed, the differences in the normalized crack penetration depths are generally about 0.10 to 0.15, and the differences appear to diminish as the aspect ratio increases. As previously noted, it is currently difficult to estimate what reasonable values of contact tensile strength might be, but the numerical results presented here suggest that further investigation into this issue is unwarranted because the critical compressive (UCS) strength is insensitive to the sidewall tensile contact strength assumption.

Figure 7 shows results from 13 individual modelling experiments with different aspect ratios and a best-fit quadratic equation. Although the determined fitting equation has an excellent coefficient of determination ($R^2 = 0.9983$), given the precision of these numerical experiments, it is appropriate to simplify this fitting equation to the following:

$$\left(\frac{UCS}{\gamma d}\right)_{SF=2} = 3\left(\frac{L}{d}\right)^2 - 2\left(\frac{L}{d}\right) + 6 \qquad \text{Equation 3}$$

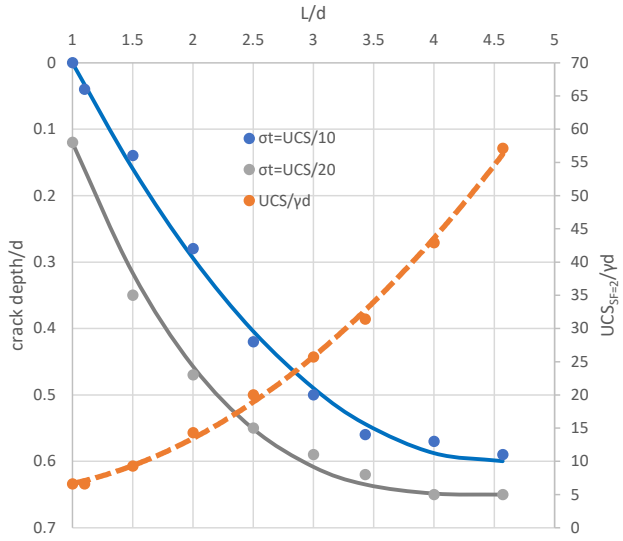

Figure 6. Sensitivity of normalized strength and normalized crack penetration depth to assumed contact tensile strength (UCS/10 and UCS/20).

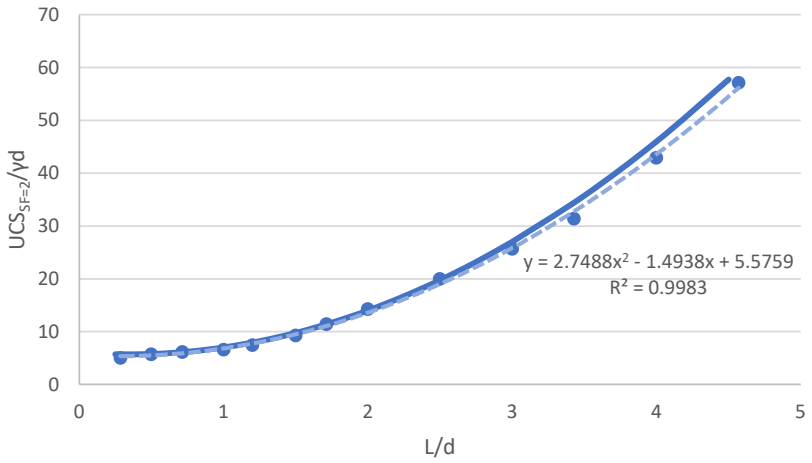

Figure 7. Fitting equation interpolating normalized strengths.

Influence of beam aspect ratio upon mechanics of failure

As previously noted, principal stress magnitudes are not presented in Figure 5 as they scale with absolute beam size. Indeed, the influence of the backfill beam's aspect ratio is shown graphically in the SF plots in Figure 8 for backfill beam aspect ratios of 0.5, 1.0, and 2.0. As previously mentioned, for aspect ratios ≤ 1.0 there is no sidewall cracking, and the stress concentration near the lower sidewall contact dictates the compressive strength requirement which is essentially the same although more localized as the aspect ratio diminishes from 1.0.

For aspect ratios increasing above 1.0, the compression zone of interest moves up towards the crack tip, and the bottom centre span tensile zone is sub-critical. At an aspect ratio ~ 2.0, the bottom tensile zone has about the same SF as the sidewall compression zone, but as previously mentioned this will be accompanied by minor vertical cracking that will result in stress relief of tension in this area without significantly affecting the compression zones elsewhere. Models were run with aspect ratios up to 4.5 for sake of comparison with published case histories (considered next). However, these extremes would not generally be recommended in practical design because the center span tensile zones become increasingly deep, the sidewall cracking becomes extensive leaving very modest contact area for the sidewall compression zone. As such, the constrained geometry for the internal arch makes stability more sensitive to any internal strength variations or inconsistencies. Practical design considerations for this limiting span will be considered later.

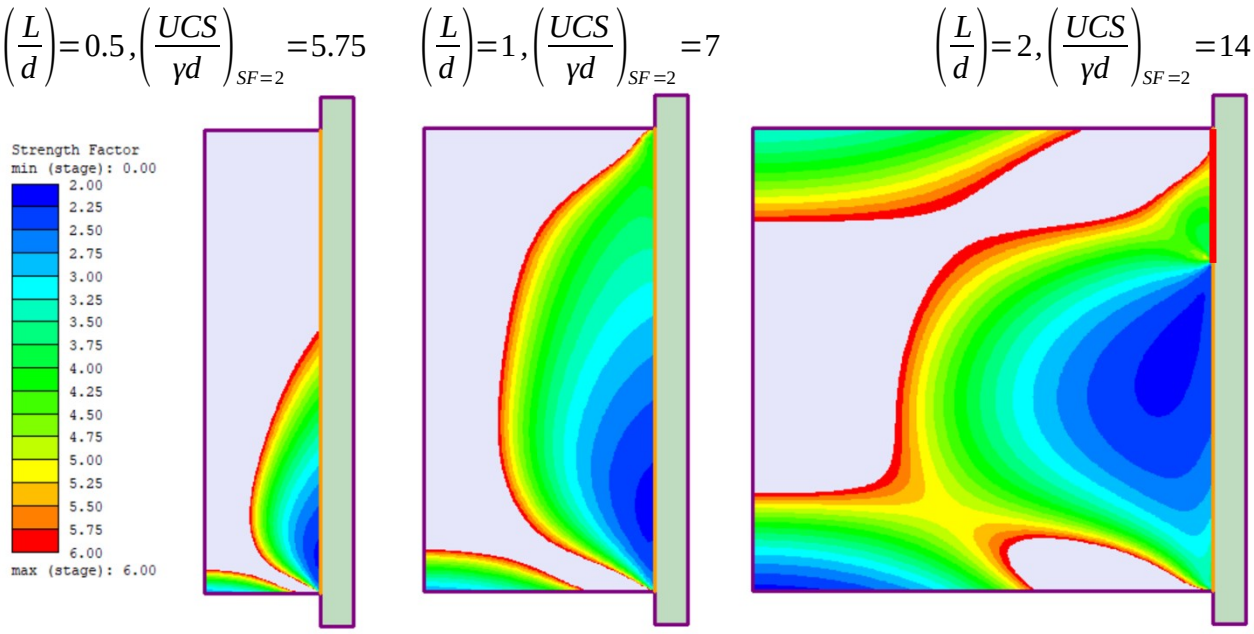

Figure 8. SF plots for beams with different aspect ratios.

Case history comparisons

Pakalnis et al. (2005) produced a database of undercut backfill case studies. The database contains data from 16 sites, some with multiple sub-cases for a total of 31 entries. Two of these sites use Cemented Hydraulic Fill while the rest of the entries are evenly split between CPB and CRF. The individual entries are also annotated to indicate if there are weak host rock mass conditions (RMR < 15, and RMR 15–25), and if there are high stress conditions typically associated with rock bursting. Figure 9 shows a comparison of the case histories with the numerical modelling strength assessments based on Equation 3, and with results obtained using Mitchell's original equation with SF = 2 and with the ratio of UCS to contact tensile strength equal to 10. Note that the modelling assumes the contact tensile strength is as low as 5% UCS (UCS/20).

Both methods (i.e. Numerical modelling and Mitchell's approach) give similar strength assessments when the backfill beam's aspect ratio is around 1 (and UCS = $7\gamma d$), but recall (Figure 6) that at this aspect ratio sidewall separation only just begins. For lower aspect ratios (i.e., $d > L$) the Mitchell's assessed strengths go to zero which is clearly unreasonable, but from the modelling results the required strength remains relatively stable (Figure 7).

For aspect ratios > 1.0, the differences between Mitchell's equations and the modelling results become increasingly large. This is because the Mitchell analysis does not account for progressive failure, whereas the modelling has incorporated this effect. This inherent problem with the Mitchell equation cannot be corrected using different contact tensile strength assumptions, even including a contact tensile strength as high as UCS/4, which is implausible.

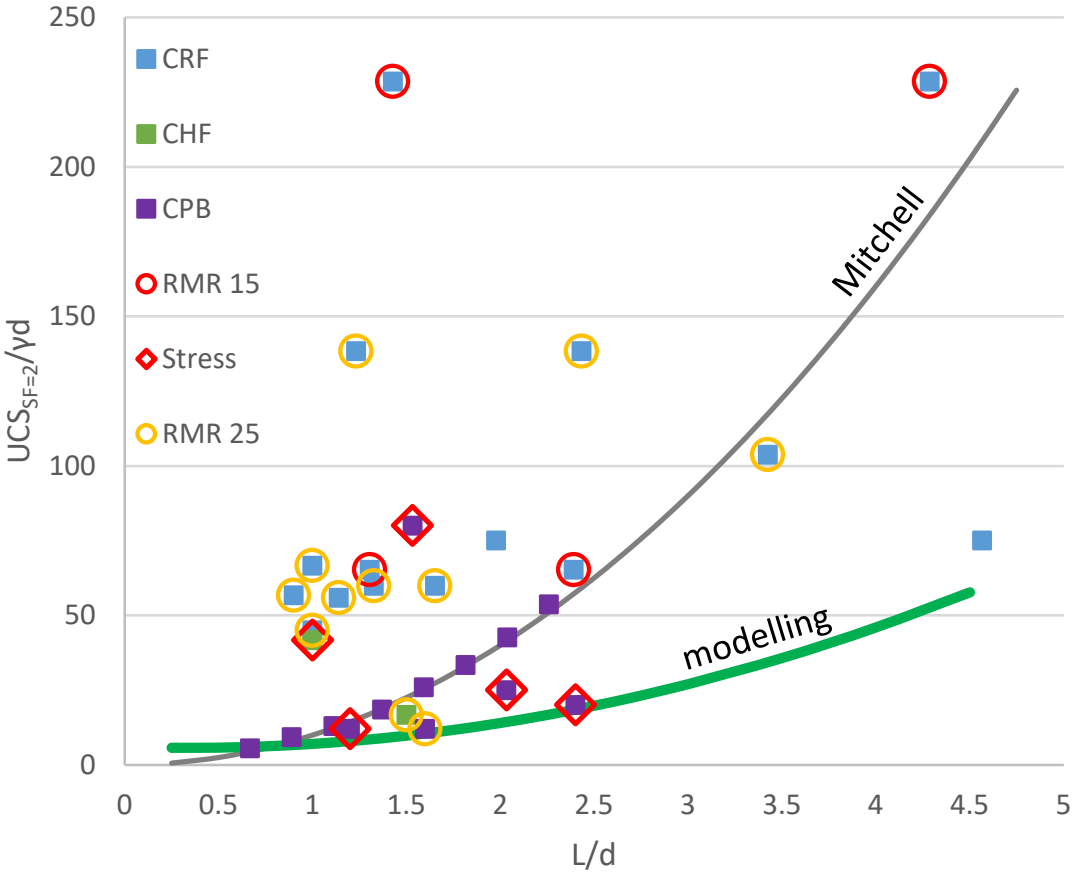

Figure 9. Comparison of case histories and results using Mitchell's equation and modelling results/

It is significant that the modelling trend captures all the lower-bound entries from the Pakalnis dataset. This includes case histories for all backfill types, for high stress situations, and for entries involving host rocks with RMR < 25. Nevertheless, most of the entries have values much larger than indicated by modelling, even though the modelling incorporates SF = 2. This could be due to one or more of the following reasons:

1. Paste strengths are commonly cited as the 28 day strengths, whereas the modelling assessed values are intended as strengths achieved when the backfill is undercut. For example, some mines might have cited the 28 day strength but then undercut much earlier and so the backfill strength at the time of undercutting was lower than the cited strength.
2. Some mines cite the average value of their strengths but have high variability in their routine UCS testing. For example, they may design according to the lower quartile of tested strengths, thus

nominally use a higher strength backfill to ensure within the as-placed backfill the variable strengths generally remain suitably higher than the design requirements.

3. The Stone (1993) and Pakalnis (2005) design charts indicate SF = 2 has been used (although specifying any SF cannot be done with confidence if the underlying method is not based on credible mechanics), but some mines may seek a higher SF especially if personnel re-enter the undercut. To this point, it should be noted that pre- or post-support should additionally be used within the backfill to prevent potential detachment of backfill blocks should horizontal weak planes be present, which could happen in the case of paste backfill with an unplanned break in the pour period, or if ponded water occurs for any reason during filling (see Donovan et al. (2007) for examples of pre-support alternatives). Because stronger backfills are also stiffer (Figure 3), there is a tendency to believe that stronger backfills will better resist wall closure. This was the basis of the 'crushing' condition discussed in the Introduction and proposed in Mitchell and Roettger (1989), although as previously noted, this condition was not used by Mitchell in the later (1991) journal article.

Additional context is required to address the question of backfill stiffness influencing wall closure. The backfill beam's axial stiffness may be approximated by AE/L (where A is the out-of-plane cross sectional area, E is Young's modulus, and L is the beam span) according to standard beam-column theory. However, the equivalent rock mass stiffness at the interface is much more difficult to ascertain because it is influenced by the entire rock mass system surrounding the mined (and backfilled) excavations. Note that some of the strongest and stiffest backfill reported in the literature is at Lucky Friday mine (Figure 2) and yet fieldwork at the mine demonstrated increasing wall closure with successive undercuts, accumulating to > 15% strain across the backfilled span (Seymour et al., 2017; Rafaldi et al., 2019).

Tested UCS samples typically fail at 1–2% axial strain and so attempting to 'design' the backfill stiffness to prevent wall closure using a simplified one-dimensional analysis may be futile. For backfill to be effective at providing a reaction to the host rock it must be confined. For example, Jafari et al. (2020) show that Williams Mine CPB with a nominal 1 MPa UCS, when tested in one-dimensional compression, provides an almost immediate 2 MPa reaction and will generate over 20 MPa reaction at 15% axial strain (Figure 9). Therefore, for the backfill to perform the role of global rock mass support, which results in Figure 10 suggest backfills can do very effectively, it must first survive being undercut. Analysis and design processes for undercut strength requirements incorporating closure do not yet exist to carry out this design task confidently, although it is noted that Sainsbury and Urie (2007) document a novel approach using a case study.

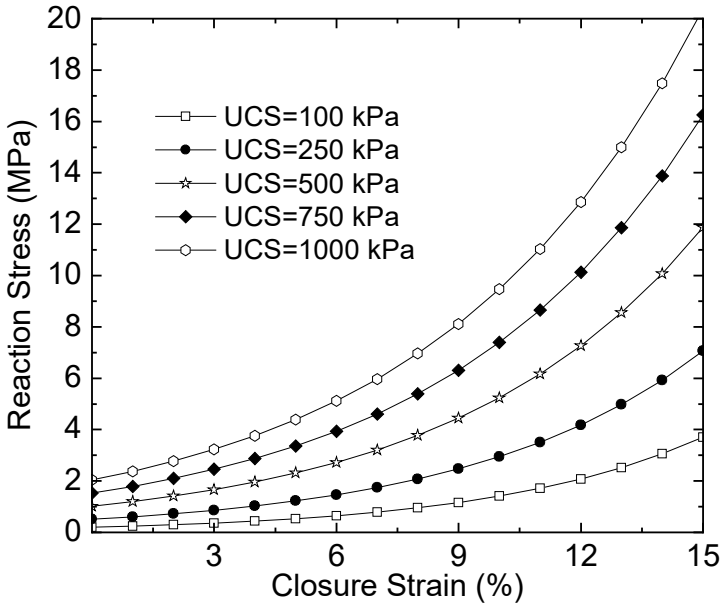

Figure 10. Backfill reaction curves obtained from one-dimensional compression testing (from Jafari et al, 2020).

Analysis limitations

The limitations to the analysis presented here should be considered when practical design approaches are being developed or used in practice, including the following:

- Vertical sidewalls were assumed. This is probably appropriate for modestly sub-vertical orebodies but sensitivity to dip angle can be investigated following the modelling approach outlined in the paper.
- No surcharge on top of the beam was considered. However, the results were normalized using the beam's unit weight. If a uniform surcharge is estimated (for example, using results from our companion paper on elastic arching) then the unit weight can be modified to take the surcharge into account.
- The intact backfill strength was parameterized assuming friction angle $\phi = ¿37°$ for which $\sigma_t = c = ¿¼$ UCS. The sensitivity of the suggested design strength to other friction angles can be investigated following the analysis approach outlined in this paper.
- The sidewall interface assumes contact shear strength is equal to the backfill's intact strength, and contact tensile strength is equal to 5% of the backfill's intact UCS (ie, UCS/20).
- The intact backfill stiffness (Young's modulus) was parameterized using $E = 10^2 \times$ UCS. This is not important, as it only influences modelled displacements which are not relevant to design given the other assumptions made.
- Sidewall closures were not considered. Small sidewall closures leading to modest equivalent axial strain (eg, about half of the strain at failure in unconfined compression testing) could lead to

increased stability by suppressing the sidewall crack development. However, more extensive closure strains on undercutting could lead to crushing failure and subsequent caving of the failed material. If this is to be analysed then the nonlinear elastic backfill stiffness should be incorporated in the analysis, which has not been considered to our knowledge in rational analysis and design procedures to date.

- Potential sub-horizontal weakness planes are not considered and if these form, they could lead to block detachment on undercutting. Pre- or post-support of the backfill beam should be considered mandatory if personnel access the undercut areas.

Conclusions

Subject to the limitations just noted, the following conclusions are drawn:

- Mitchell's original flexure criterion is too simple for high aspect ratio beams where required strength is over-predicted. This is because the method only considers the onset of sidewall failure at the upper corners, and this is not commensurate with structural collapse of the backfill beam.
- Numerical analysis must be used to model the backfill beam's progressive failure process as the sidewall cracking increases. The work presented here favours using joint elements to represent this interface behaviour and emphasizes the need to calibrate the joint's normal stiffness to achieve the theoretically correct tensile stress concentration at the sidewall's upper corner when the model is run as elastic (ie, no joint failure).
- Backfill beams with aspect ratios ≤1 (ie, $L \leq d$) do not undergo sidewall cracking. The critical stress concentration is in compressive zones near the bottom sidewall contact. Avoiding sidewall detachment is inherently safer, and it is therefore recommended that undercut backfills should have approx equal spans and heights wherever possible.
- As a backfill beam's aspect ratio increases (ie, $L > d$ ¿ up to about $L = 2d$), sidewall cracking gets progressively deeper, but the critical stress concentration remains a compression zone at the sidewalls.
- For aspect ratios > 2 (up to a maximum 4.5 investigated here) a tensile zone develops at the backfill beam's center span bottom face. However, this results in vertical tensile cracks propagating upward into a compression zone where they are stabilized. Therefore, the critical stress concentration remains the compressive zones at the sidewalls.
- A normalized equation for predicting required backfill strength with SF = 2 is proposed based on numerical modelling results.
- The proposed normalized predictive equation is an improvement on previous methods in that it gives reasonable strengths for low aspect ratio beams ($L \ll d$) whereas previous methods predict required strengths approaching zero; and, as the aspect ratio increases, the predicted required strength becomes less than previous methods.
- The proposed equation's results are consistent with the lower bound strengths determined from field case studies, and these studies contain all common fill types, backfills in weak host rocks, and backfills in high ground stress conditions.

Finally, the number of available published case histories is relatively small, and it would be beneficial to expand the case history database to gain confidence in all analysis and design methods used for undercut backfill design challenges.

Acknowledgements
The authors acknowledge the support of Paterson & Cooke Canada Inc. in the preparation, publication, and presentation of this work at Minefill 2024, including very useful conversations with Andy Beveridge and Paul Carmicheal. The first author acknowledges the direct and in-kind support of Agnico Eagle Mines Limited and the Macassa mine in a related ongoing research program at the University of Toronto.

References

Donovan, J., Dawson, J. and Bawden, W.F. (2007) David Bell Mine underhand cut and fill sill mat test. In, Proceedings of the 9th International Symposium in Mining with Backfill, Montréal, 2007 Apr (Vol. 29).

Jafari, M., Shahsavari, M. and Grabinsky, M. (2020) Cemented paste backfill 1-D consolidation results interpreted in the context of ground reaction curves. Rock Mechanics and Rock Engineering, Vol 53, pp. 4299-308. https://doi.org/10.1007/s00603-020-02173-5

Grabinsky, M., Jafari, M., and Pan, A. (2022) Cemented Paste Backfill (CPB) Material Properties for Undercut Analysis. MDPI Mining Journal, Special Edition on Application of Empirical, Analytical, and Numerical Approaches in Mining Geomechanics. Vol. 2, No. 1, pp. 103-122. https://doi.org:10.3390/mining2010007

Grabinsky, M.W. and Thompson, B.D. (2024) Elastic Arching Effects in Tall Cemented Paste Backfilled Stopes. In, Proceedings of Minefill 2024, 12-15 May, Vancouver (this volume).

Mitchell, R. (1991) Sill mat evaluation using centrifuge models. Mining Science and Technology, Vol. 13, pp. 301-313. https://doi.org/10.1016/0167-9031(91)90542-K

Mitchell, R.J., and Roettger, J.J. (1989) Analysis and modelling of sill pillars. In, Innovations in mining backfill technology, London: CRC Press, pp. 53-61.

Pakalnis, R.; Caceres, C.; Clapp, K.; et al. (2005) Design spans - underhand cut and fill mining. In, Proceedings of the 107th CIM-AGM, Toronto, pp. 1-9. www.cdc.gov/niosh/mining/userfiles/works/pdfs/dsuca.pdf (accessed 2022-02-05)

Raffaldi, M.J., Seymour, J.B., Richardson, J., Zahl, E. and Board, M. (2019) Cemented paste backfill geomechanics at a narrow-vein underhand cut-and-fill mine. Rock Mechanics and Rock Engineering, Vol. 52, pp. 4925–4940. https://doi.org/10.1007/s00603-019-01850-4

Sainsbury and Urie, Stability Analysis of Horizontal and Vertical Paste Fill Exposures at the Raleigh Mine, International Symposium on Minefill, (Minefill 2007), Paper 2527.

Seymour, J.B., Rafaldi, M.J., Abraham, H., Johnson, J.C. and Zahl, E.G. (2017) Monitoring the in situ performance of cemented paste backfill at the Lucky Friday Mine. In, The 12th International Symposium on Mining with Backfill, Denver, pp 19–22.

Starfield, A.M. and Cundall, P.A. (1988) Towards a Methodology for Rock Mechanics Modelling. International Journal of Rock Mechanics and Mining Sciences & Geomechanics Abstracts, Vol. 25, No. 3, pp. 99-106. https://doi.org/10.1016/0148-9062(88)92292-9

Stone, D. (1993) The optimization of mix designs for cemented rockfill. In, Proceedings of Minefill 93, Johannesburg: SAIMM pp. 249-253.

Vick, S. (1990) Planning, Design, and Analysis of Tailings Dams. Vancouver: BiTech Publishers Ltd. 369 p. https://open.library.ubc.ca/media/download/pdf/52387/1.0394902/5 (accessed 2023-12-10)

Yang, L., Hou, C., Zhu, W. and Li, L. (2024) Effect of roughness on shear behavior of interface between cemented paste backfill and rock. Construction and Building Materials, Vol. 411, https://doi.org/10.1016/j.conbuildmat.2023.134312